Applied Energy 323 (2022) 119546

Contents lists available at ScienceDirect

Applied Energy

journal homepage: www.elsevier.com/locate/apenergy

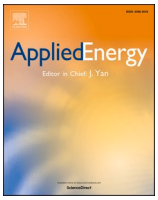

A PV ramp-rate control strategy to extend battery lifespan using forecasting

A. Gonzalez-Moreno *, J. Marcos, I. de la Parra, L. Marroyo

Dept. of Electrical, Electronic and Communication Engineering, Public University of Navarra (UPNA), Campus Arrosadia, Edificio los Pinos, 31006 Pamplona, Spain

HIGHLIGHTS

- A ramp-rate control strategy is proposed to use minimum storage and reduce battery degradation.
- The proposal and three benchmark strategies are simulated with 2-year real data of a multi-megawatt PV plant.
- PV power forecasting, based on real publicly-available numerical weather prediction (NWP) series, is used to reduce battery cycling degradation.
- Levelized cost of energy (LCOE) analysis shows that the proposed strategy is the most cost-effective among the evaluated techniques.

ARTICLE INFO

Keywords:
PV fluctuations
PV smoothing
Ramp-rate limitation
Energy storage Systems (ESS)
PV integration
Levelized Cost of Energy (LCOE)

ABSTRACT

This study analyses and presents a new ramp-rate control algorithm for smoothing PV power fluctuations, designed to address three fundamental objectives: to reduce battery cycling, to meet minimum storage requirements and to be able to operate, without ramp-rate violations, with real publicly-available forecasting. The algorithm was compared to three benchmark methods and, as a performance limit, also to a hypothetical perfect prediction. Different performance variables were analyzed for all the strategies within a restricted ramp-rate constraint (2%/min): minimum storage requirement, battery power distributions, throughput energy, state of charge (SOC) distributions, degradation (calendar and cycling), expected battery lifespan and levelized cost of energy (LCOE). The proposal proves to be the most cost-effective smoothing technique and the simulation results show that its performance is comparable to the obtained with the use of an assumed perfect prediction.

1. Introduction

Over the past decade, the photovoltaic (PV) power has increased dramatically worldwide. In fact, the global PV power capacity has increased more than 5000% between 2007 and 2018 [1]. At present, utility scale PV production is one of the most cost-effective generation technologies in terms of the levelized cost of energy (LCOE) [2,3,4]. For this reason, this growth pattern is expected to continue in the future. There are regions in which the increase of PV power has led to a significant increase in the ratio between solar and conventional power generation. This can produce issues related with the characteristic intermittency of the solar resource, in special during cloudy scenarios [5,6]. The ratio of change of the PV plant's power output mainly depends on the cloud speed and the PV covered area [5,7,8,9]. Output power variations of up to 90%/min were reported for different locations and plant sizes [7,10,11,12]. Power fluctuations these type can produce grid quality problems related to frequency or even voltage stability [6,13,14,15]. As a result, different transmission system operators (TSOs) have established regulations limiting the maximum permitted rate of change for PV plants [16,17,18,19,20]. The range in which the ramp-rate (RR) limit is tolerated can vary between 1%/min, in the case of the most restrictive scenario in Mexico [17], to 10%/min, according to the Puerto Rican grid code [16]. The traditional approach to smooth PV fluctuations is to install an energy storage system (ESS) which can include: flow-batteries, super capacitors, fuel cells, Li-ion batteries or a combination of them [21]. Li-ion batteries are the most suitable ESS technology thanks to their technical development, performance [22] and expected price reduction [23]. All the same, the introduction of an ESS increases the initial investment of the project and the total cost of the generated energy [3,24,25]. Therefore, it is essential to minimize the additional cost incurred by the use of batteries in order to limit the loss of competitiveness in the PV LCOE. The increased LCOE depends on two main factors: the initial cost of the EES and the battery lifespan. As will be shown, the intrinsic characteristics of every ramp-rate strategy have considerable impact on both these factors.

Among the different smoothing strategies the most commonly

* Corresponding author.
E-mail address: alejandro.gonzalez@unavarra.es (A. Gonzalez-Moreno).

https://doi.org/10.1016/j.apenergy.2022.119546
Received 18 October 2021; Received in revised form 3 June 2022; Accepted 24 June 2022
Available online 6 July 2022

studied [26] are the classical ramp-rate control [27] and the moving average filter [24]. The first one (hereinafter Strategy 0) permanently evaluates the PV power variation and charges/discharges the ESS when the desired smoothing is exceeded. Due to the fact that the sign of the next fluctuation is unknown, the battery must have the capacity to absorb/dispatch, at any time, the corresponding energy to the worst positive/negative fluctuation that can take place [9]. Therefore a stored energy control loop is required with the reference set at 50% and a minimum capacity that is twice as high as the energy associated with the worst-case fluctuation [9].

The moving average filter (hereinafter Strategy 1) injects the mean value of the PV power during a prefixed time window (introducing a fixed delay). The ESS handles the difference between the injected and PV power; as a consequence of the delay, the storage equipment permanently cycles, and produces at least one deep cycle per day; however, the strategy demands a storage capacity close to half that of Strategy 0 [28].

With the aim of combining the advantages of strategies 0 and 1, i.e. non-intensive use and low storage requirements, [10] proposed the clear sky-dark sky technique (hereinafter Strategy 2) which is able to operate with the minimum storage established in [9]. The strategy uses the production limits of the PV plant, namely clear and overcast sky conditions, and establishes the storage required to smooth possible maximum upward and downward fluctuations, i.e. from the instantaneous operating point to estimated clear and overcast sky conditions. In this way, the strategy modifies the energy stored in the battery in order to attenuate both these fluctuations.

On the other hand, forecasting-based ramp-rate control strategies with no ESS have been proposed [29,30,31]. These change the plant operating point in advance, in a desirable way, e.g. with constant RR. If the forecast is completely accurate, it has been demonstrated that the energy wastage is low even for exigent smoothing requirements [32]. Nevertheless, the current high-resolution and intrahour forecasting techniques are far from this goal.

However, PV power forecasting can be used to improve existing ESS dependent strategies. For example, Strategy 2 permanently makes a constant assumption of the worst-case scenarios, therefore, the strategy controls the battery in a pessimistic manner, preparing it, in many cases, for possible but nonexistent fluctuations, producing unnecessary cycling. This paper presents a control technique that outperforms Strategy 2 by limiting the expected fluctuations considering not only the clear and overcast limits, but also the predicted PV power. The proposed strategy is compared to other technics already proposed in bibliography, taking into account different performance parameters: minimum storage requirement, battery power distribution, throughput energy, state of charge (SOC) distribution, calendar degradation (*CaD*), cycling degradation (*CyD*), expected lifespan and levelized cost of energy (LCOE). The simulations were carried out with real 5-second PV power production series and a real 1-hour publicly-available (costless) Numerical Weather Prediction (NWP) based forecast. The improvement is achieved through a significant reduction in ESS cycling, thereby extending the battery lifespan.

A description of the data used is provided in Section 2, the minimum storage requirements are discussed in Section 3, the three benchmark strategies are briefly described in Section 4, the proposal strategy is presented and analyzed in Section 5, the comparison with benchmark strategies is carried out in Section 6, and the conclusions are set out in Section 7.

2. Experimental data

The PV power series is a 5-second sampled PV production recorded at the Amaraleja PV plant (38°11′20″N, 07°12′08″0W) in the course of two years. The plant comprises 2520 vertical solar trackers with a tilt angle of 45°, the covered area is 250 ha and the ground cover ratio (GCR) is 0.162. The peak plant power is 45.6 MW and the inverter rated power (P^*) is 38.6 MW.

The forecast used (*FC*) was a series based on a parametric plant model [33] that uses as inputs the results of a publicly-available (costless) Numerical Weather Prediction (Meteogalicia's THREDDS server), which has a spatial resolution of 12x12 km, a temporal resolution of 1 h, covers the region delimited by 21.58° W to 6.36° E and 33.64° N to 49.57° N and uploads its methodological forecasting every six hours. The *FC* values obtained were placed at the beginning of each hour and then interpolated with the purpose of fitting them to the simulation time step (5s).

3. Minimum storage requirement for ramp-rate control

A key feature of any RR control strategy is the required storage. The minimum required capacity was data-based established in [9] and has been validated for different plant sizes (from 550 kW to multi-megawatt plants) and for different geographical regions (separated by more than 500 km) [9], which allows the generalization of the results to different plant sizes and geographical locations. The amount of required energy (E_{wf}) is estimated with the model of the worst fluctuation (Fig. 1). This depends on the desired ramp restriction (r), the maximum expected power change (ΔP_{max}) and the PV plant dimensions and is independent of the geographical coordinates of the plant [9]. The PV power (P_{pv}) fluctuation is modelled as an exponential decay with time constant τ, the injected power (P_g) must vary with constant slope (r), the difference between them must be provided by the battery (P_b). The amount of energy that must be provided by the battery, which is equal to the integral of P_b, can be calculated, in per unit, as follows:

$$E_{wf} = \Delta P_{max}\left(\frac{\Delta P_{max}}{2r} - \tau\right) \tag{1}$$

The time constant τ and the shortest dimension have been related in [9]:

$$\tau[s] = 42 \cdot L[\text{km}] - 0.55 \tag{2}$$

The worst fluctuation occurs in central daytime, when a cloud front covers (or leaves), at high speed, the PV plant following the direction of its shortest dimension (L).

Once the storage capacity is determined, it is then possible to relate stored energy and state of charge (SOC), a crucial parameter in battery management. Taking into account the fact that capacity expressed in terms of charge (C_b [Ah]) and energy (C_b [kWh]) maintain a liner correlation during the whole life of batteries [34], it is possible to use the energy instead of charge to avoid the need of a detailed battery model and to permit much faster long-term simulations:

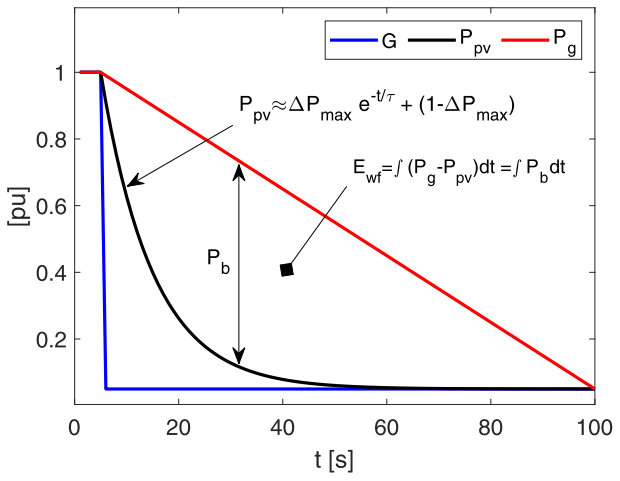

Fig. 1. Worst fluctuation model. G: Irradiance at a single point, P_{pv}: PV power, P_g: injected grid power with ramp-rate compliance.

$$SOC(t) = \frac{Q(t)}{C_b \ [\text{Ah}]} \approx \frac{\int \eta^{sign(P_b)} P_b \cdot dt \ [\text{kWh}]}{C_b \ [\text{kWh}]} \quad (3)$$

For this reason, despite the fact that SOC and stored energy are not exactly equivalent, in the subsequent sections they are used indistinctly.

4. Benchmark strategies

In general, all PV RR strategies with battery have the same generic schema (it can be seen in Fig. 2), what differs from one strategy to another is the algorithm that determines the battery power (P_b) and the additional requirements to be able to function: additional measurements, communications, forecasting, database consultation, etc.

With the aim of comparing the performance of the proposed method, three representative control strategies were also simulated: classical ramp-rate control (Strategy 0), the one with minimum cycling degradation [27]; mean average method (Strategy 1), the most extensively used in the bibliography[26]; and clear sky-dark sky technique (Strategy 2), which permits the use of the minimum storage [9] and is the origin of the proposal. They are summarily described below.

4.1. Strategy 0: Classical ramp-rate control

This strategy modifies the power injected into electric grid (P_g) during each sampling period, in such a way that its rate of change does not exceed a predefined RR limit (r), i.e. during P_{pv} ramp violations, P_g evolves in a straight line with a constant gradient r [27]:

$$\left|\frac{\Delta P_g}{\Delta t}\right| \leq r \quad (4)$$

The complete control diagram is presented in Fig. 3(a). The excess or lack of power between P_g and P_{pv} is P_b, and must be handled by the battery. A SOC control loop with the reference (E_b^*) set to half the capacity is required; firstly, due to a discharge tendency during certain sky conditions and, secondly, to guarantee that at any time the battery can absorb or inject E_{wf} [9]. Therefore, the minimum battery capacity ($C_{0,\min}$) should at least be [27]:

$$C_{0,min} = 2 \cdot E_{wf} \quad (5)$$

The loop is completed with a proportional controller that sets the power (P_Δ) needed to reach the reference. The difference between P_{pv} and P_Δ, which is the desired injected power (P_g^*), should be limited in order to achieve the required ramp-rate (r).

The aim of this control method is to only use the battery when needed, e.g. when the ramp-rate (r) is violated. As can be seen in Fig. 3 (b), this control method does not cycle the battery in excess, even on days with severe power fluctuations. As a result, the battery degradation will be low and, consequently, the battery lifespan is expected to be longer (discussion in section 6, strategies comparison and specific results in Table 5). However, as it is evidenced in (eq.5), the minimum capacity is twice that required for the worst fluctuation and, as a consequence, the expected purchase cost is high.

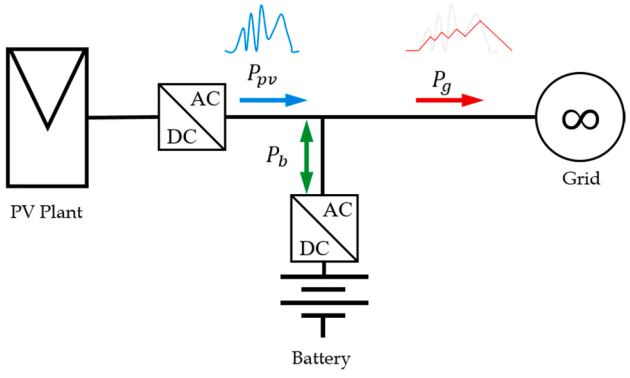

Fig. 2. Schematic diagram of a PV plant with battery storage and smoothing capabilities connected to the grid.

4.2. Strategy 1: Mean average filter

The moving average method is the most representative strategy among the filter-based ones [26]. The control diagram is shown in Fig. 4 (a). Injected grid power (P_g) is calculated as the mean of P_{pv} over a predefined period of time (T). The battery absorbs or injects power (P_b) in order to manage the difference between the P_{pv} and P_g. The requirements of this method were analytically established in [28]. In order to obtain a desired ramp limit (r), the length of the window (T) must be at least:

$$T = \frac{\Delta P_{max}}{r} \quad (6)$$

Furthermore, the minimum capacity ($C_{1,min}$) is [28]:

$$C_{1,min} = \frac{\Delta P_{max}}{2}(N-1) \cdot \Delta t \quad (7)$$

where N is the number of time samples included in the time window and Δt is the sampling period.

The merit of this strategy over Strategy 0 is that requires nearly half of its capacity. However, as is evident when Fig. 4(b) is compared to Fig. 3(b), the battery is excessively cycled due to the intrinsic over smoothing introduced by the moving average [26,27].

Moreover, because of the delay between P_g and P_{pv}, the battery suffers a complete deep cycle even during clear days, resulting in a shorter expected lifespan.

4.3. Strategy 2: Clear sky-dark sky method

For the purpose of including the advantages of strategies 0 and 1 (reduced cycling and reduced storage requirements) and mitigating their disadvantages (substantial storage requirements and severe cycling), the clear sky-dark sky ramp-rate control was proposed [10]. Its main goal is to permit implementation with the minimum capacity (E_{wf}, eq.1)

$$C_{2,min} = E_{wf} \quad (8)$$

The control scheme is basically the same as Strategy 0 (Fig. 3(a)), however, the SOC reference (E_b^*) is not a fixed value. Instead, the reference is uploaded for each sampling time based on the difference between the current power (P_{pv}), and the upper and lower practical production limits, clear sky (P_c) and dark sky (P_d) conditions (Fig. 5(a)). The method to estimate P_c is detailed in [10] (we used as input for the global horizontal radiation the historical data available in [35]), P_d can be approximated as a small percentage of P_c, in this study 5% is used.

By using the fact that the magnitude of the maximum fluctuation is limited, at any instant, by the difference between P_d and P_c, it is possible to estimate the energy that needs to be stored. When P_{pv} is close to P_c the only possible fluctuation is negative and the severest one is approximately $P_d - P_c$ requiring a high storage level. In contrast, when P_{pv} is close to P_d the only possible fluctuation is positive and its maximum value is nearly $P_c - P_d$, therefore a low storage level is required. In any intermediate point, upward and downward fluctuations are possible, but their magnitudes are shorter ($P_c - P_{pv}$ and $P_{pv} - P_d$, respectively). There exist some instants in which P_{pv} can be higher than P_c (as can be seen in Fig. 5(b)), but these events are produced by the reflection from nearby clouds and their associated energy and frequency of occurrence are low.

The control process is described below.

In each sampling period, the values of P_c, P_d and P_{pv} are uploaded and two differences are computed (shown in Fig. 7(a)):

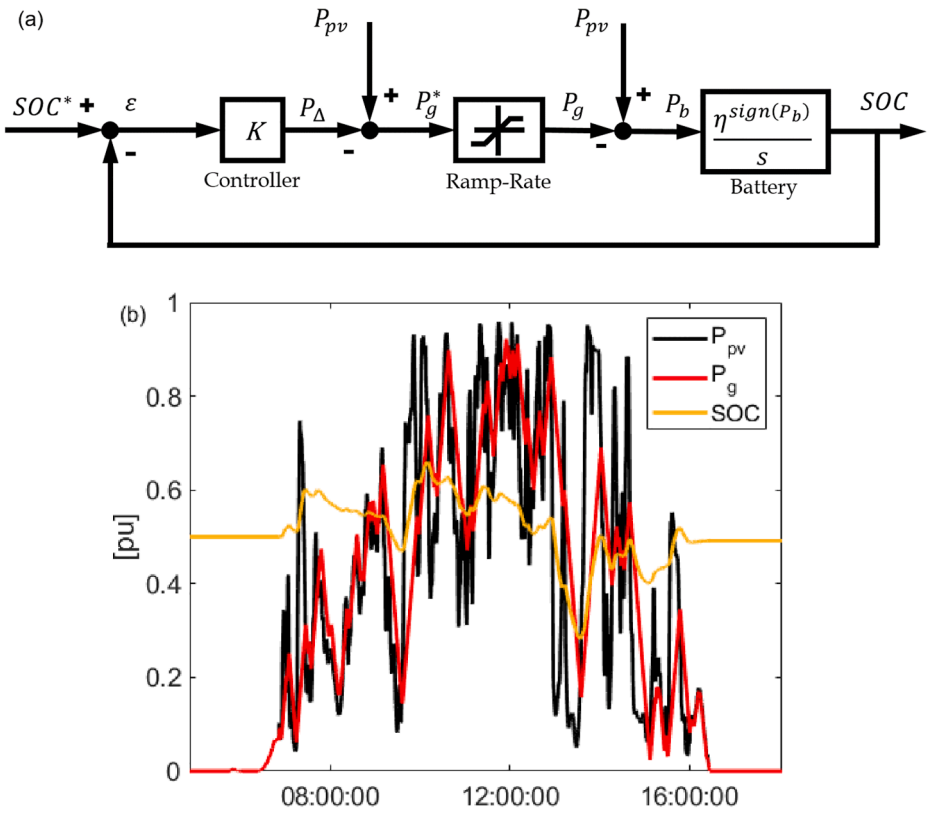

Fig. 3. Classical ramp-rate control (Strategy 0). (a) Control diagram, (b) performance example during day with severe power fluctuations ($r = 2\%$/min).

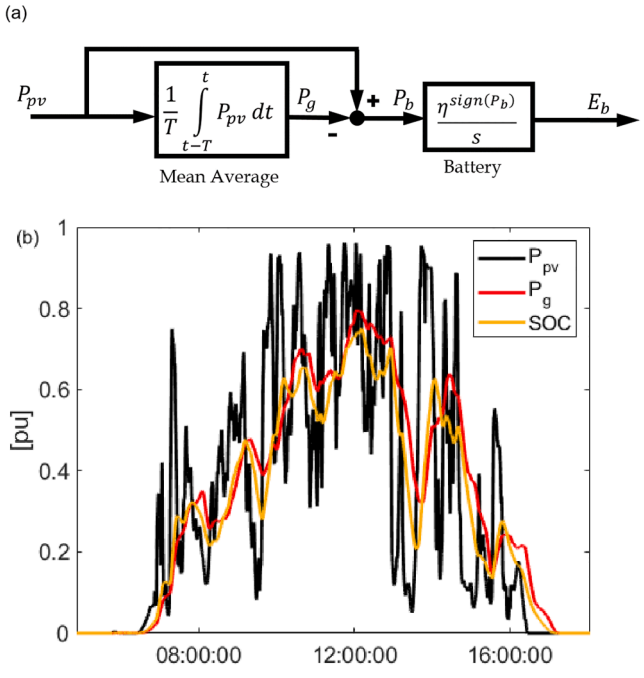

Fig. 4. Mean average control (Strategy 1). (a) Control scheme, (b) example of day with severe power fluctuations ($r = 2\%$/min).

$$\begin{aligned}\Delta^+(i) &= P_c(i) - P_{pv}(i)\\ \Delta^-(i) &= P_{pv}(i) - P_d(i)\end{aligned} \tag{9}$$

These values limit the two maximum power fluctuations that can occur at any time. By using eq.1 it is possible to estimate the energy required to smooth each one:

$$\begin{aligned}E^+ &= \Delta^+\left(\frac{\Delta^+}{2r} - \tau\right)\\ E^- &= \Delta^-\left(\frac{\Delta^-}{2r} - \tau\right)\end{aligned} \tag{10}$$

When the current SOC permits the simultaneous absorption of E^+ and injection of E^-, then the SOC reference (E_b^*) remains constant. When the battery is unable to manage one of them, then the reference is set to the proper value. The logic is described by thenext pseudo code:

$$\begin{aligned}&\textbf{if } E_b + E^+ > E_{max}\\ &\quad E_b^* = E_{max} - E^+\\ &\textbf{elseif } E_b - E^- < E_{min}\\ &\quad E_b^* = E_{min} + E^-\\ &\textbf{else}\\ &\quad E_b^* = E_b\end{aligned} \tag{11}$$

The strategy succeeds in reducing the extreme over-cycling of Strategy 1 with even less minimum storage. However, due to is pessimistic approach, the permanent assumption of the worst possible power fluctuation, there are episodes in which Strategy 2 uses unnecessarily the battery. Two particular cases have special interest, they are shown in Fig. 6. The first one occurs when a low level of energy is stored in the ESS at the beginning of the day and the sky is clear or marginally covered (Fig. 6(a)); the second one occurs when a high level of energy is stored and the sky is vastly covered (Fig. 6(b)). In these conditions, the algorithm prepares the battery to attenuate the worst possible fluctuation (according to the general power limits of the plant, even if it does not occur) and produces an unnecessary charge or discharge process. In Fig. 6(a) the initial state of the battery is low and, when solar radiation increases, the algorithm prepares the system for an eventual Sun obstruction by charging the battery, however it does not occur, producing unnecessary deep half cycle. The inverse case is shown in Fig. 6 (b), where a undesirable discharge produces another deep half cycle.

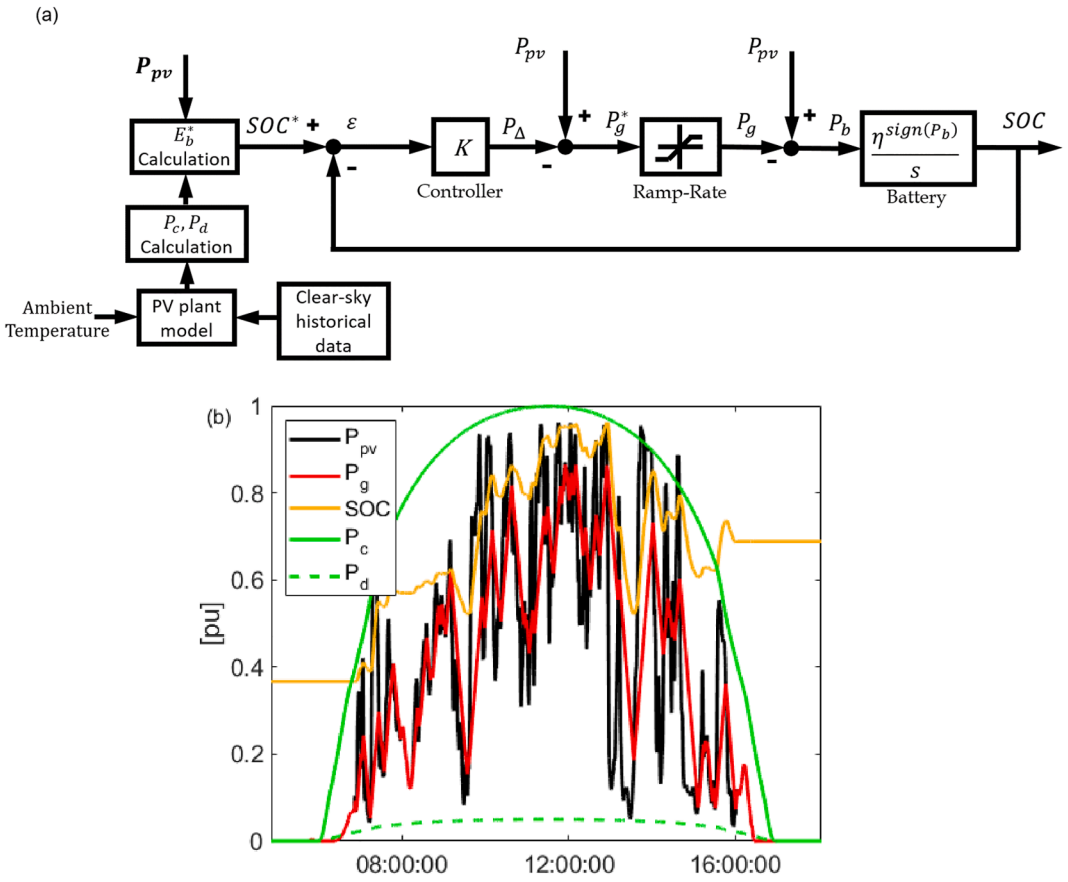

Fig. 5. Clear sky-dark sky control (Strategy 2). (a) Control diagram, (b) performance example during a day with severe power fluctuations (r = 2%/min).

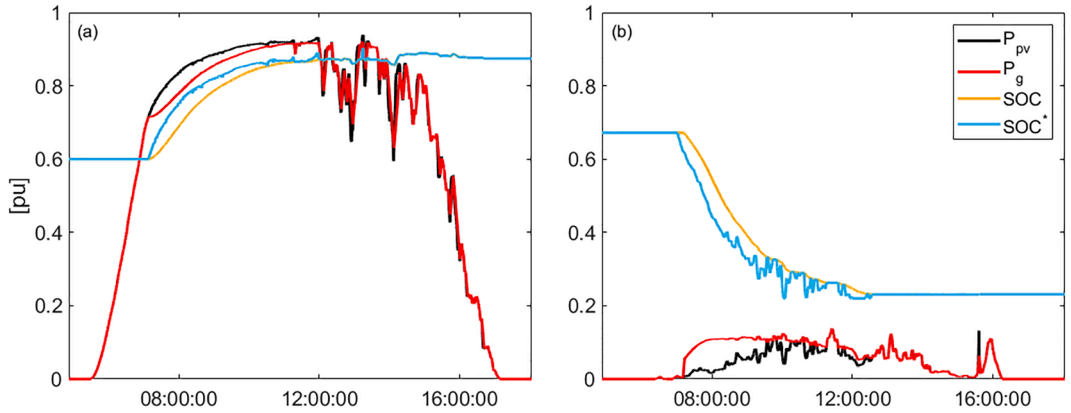

Fig. 6. Clear sky-dark sky control (Strategy 2). Over-cycling examples produced by Strategy 2. (a) Unnecessary charge, (b) unnecessary discharge. In both cases, the algorithm prepares the battery, unnecessarily, for fluctuations that do not occur.

The solution to this behavior is discussed in the next section.

5. Proposal: Clear sky-dark sky with forecasting

The proposed scheme is based on Strategy 2 but to improve some of its aspects: over-cycling due to the pessimistic assumption that the battery must be prepared to manage both instantaneous worst possible upward and downward fluctuations at any time (Eqs. (9) and (10)).

If the control could have information about the future behavior of PV power, by using a forecasting method, and following the logic of Strategy 2, it would be able to reduce the number of unnecessary changes in SOC (as in Fig. 6). As a result, it would be possible to reduce the battery cycling by taking into account forecasted PV limits instead of P_c and P_d (as in Fig. 7). Evidently, the performance of this approach is completely dependent on the accuracy of the forecasting available: if there is an overestimation of the possible fluctuation, then the cycling reduction would not be as much as it could; on the contrary, if there is an underestimation, then there would be risk of ramp-rate non-compliance.

Assuming the ideal case, perfect forecasting (FC_p), the system would modify E_b^* just when is needed, minimizing the battery cycling. With the aim of identifying the performance limit, Strategy 3 is defined.

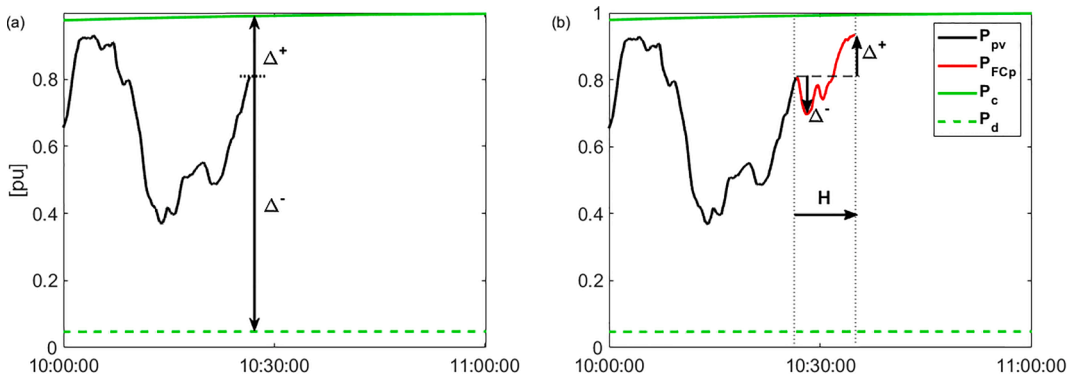

Fig. 7. General case comparison between Strategies 2 and 3. (a) Strategy 2 with its pessimistic approach, (b) Strategy 3 with perfect forecast (FC_p) and temporal horizon (H).

5.1. Strategy 3: Perfect prediction (FC_p)

In the same way as Strategy 2, Strategy 3 estimates the maximum power fluctuation that can take place in the instant i. However, instead of using the pessimistic approach of the clear and dark sky limits ($P_c(i)$ and $P_d(i)$), Strategy 3 determines Δ^+ and Δ^-, each sampling period, by taking into account present (P_{pv}) and maximum and minimum values of the forecasted production (P_{FC}), within a temporal horizon (H) with N samples. Given that, within the horizon, the extreme values of P_{FC} could be overpass the instantaneous limits of P_{pv} ($P_c(i)$ and $P_d(i)$), the calculated values of Δ^+ and Δ^- should be limited in order to avoid over-cycling. Consequently eq.9 is modified as follows:

$$\begin{aligned}\Delta^+(i) &= min\{max\{P_{FC}(i+1,\ldots,i+N)\}, P_c(i)\} - P_{pv}(i)\\ \Delta^-(i) &= P_{pv}(i) - max\{min\{P_{FC}(i+1,\ldots,i+N)\}, P_d(i)\}\end{aligned} \quad (12)$$

The subsequent steps of the algorithm remains unaltered (see subsection 4.3 Strategy 2).

A schematic comparison between strategies 2 and 3 is presented in Fig. 7. In the case of Strategy 2 (Fig. 7(a)) the value of Δ^- leads, according to Eqs. (9) and (10), to high SOC's set point, if the energy stored in the ESS is insufficient, then the proportional control will try to reach it by charging the battery (preparing the system for a potential severe downward fluctuation). However, the future path of the PV production is that shown in Fig. 7(b) and the charge produced with the logic of Strategy 2 would lead to over-cycling.

5.2. Strategy 3w: Real prediction (FC)

Considering the limitations of PV power prediction, some modifications should be made to Strategy 3 in order to avoid malfunctioning due

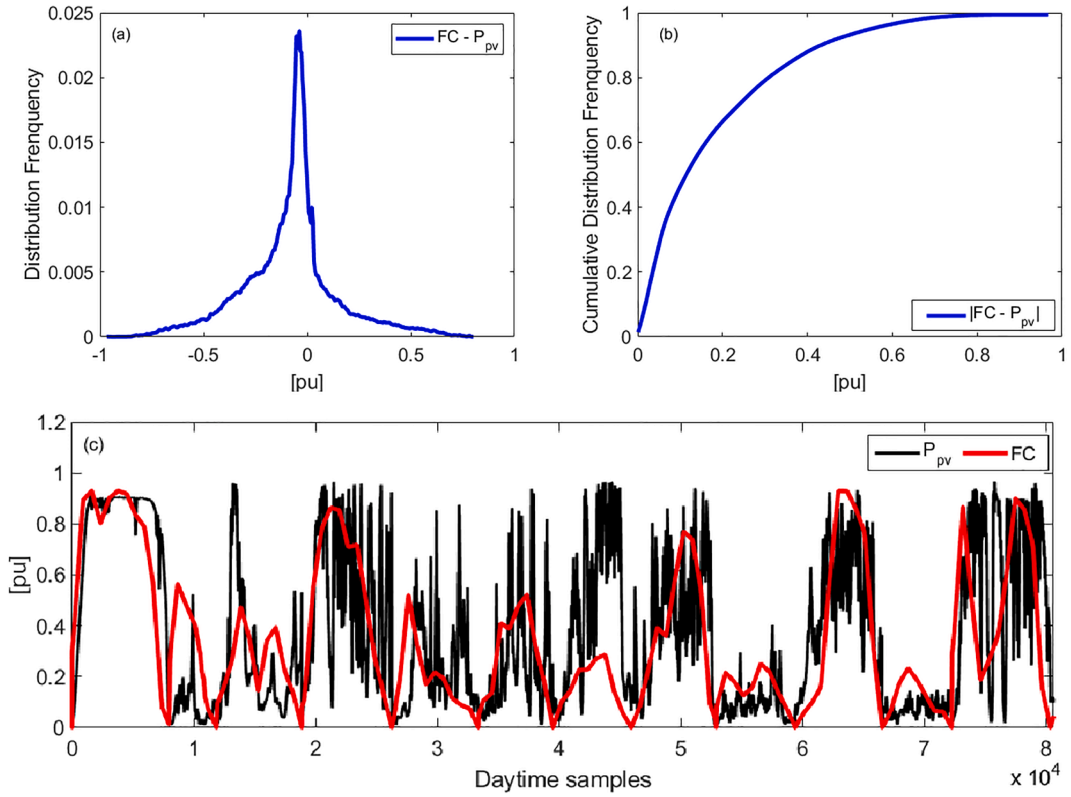

Fig. 8. NWP based PV power forecast (FC) accuracy over the entire period (2 years). (a) Error ($FC - P_{pv}$) distribution frequency, (b) absolute error ($|FC - P_{pv}|$) cumulative distribution frequency and (c) 12 consecutive days with severe power fluctuations, clear and completely overcast sky. In (c), the data corresponding to the night-time have been omitted.

to forecasting inaccuracy and to be able to work with it. The PV power forecasting in this study (hereinafter *FC*) is a publicly-available (costless) hourly Numerical Weather Prediction. The summary of *FC* performance for the two years (in 5-second sampling time) is presented in Fig. 8 and Table 1. Fig. 8 shows some frequency distributions related to *FC* error ($FC - P_{pv}$) and 12 consecutive days (omitting nighttime), while Table 1 contains different error metrics.

Fig. 8(a) demonstrates a nearly symmetrical but negative-biased distribution, with its peak value shifted −4% and a mean bias error (MBE) of −6.46% (see Table 1), which means *FC* tends to underestimate the real power.

The reader should bear in mind that this study is not focused on whether or not a forecasting method is satisfactory, and neither does it aim to develop an accurate forecasting algorithm, instead it seeks to prevent excessive cycling degradation while smoothing PV power fluctuations (and the negative economic/environmental impact of battery replacement), even if the available forecast, due to its temporal resolution, is unable to foreseen those such power fluctuations. The reduction of cycling degradation will be produced by avoiding unnecessary battery reference variations.

Given that *FC* is unable to capture the fast power transitions in intra hour horizon, as can be seen in Fig. 8, it is expected that, if used in the same way as FC_p, there will be numerous violations of the RR requirements. However, as it can be seen in Fig. 8(b), *FC*'s MAE is below 20% for 60% of the time. Certainly, that kind of information could be used by the control algorithm to improve the cycling degradation, although the overall performance would depend on its *ability* to identify those times when *FC* is reliable.

Numerical Weather Prediction, generally speaking, can accurately forecast clear and overcast days and in such cases, the forecast (like *FC*) resembles the real power production. Fig. 8(c) shows 12 consecutive days, just at daytime, and *FC* behavior. The performance during clear (1st) and fully overcast days (2nd, 9th and 11th) is satisfactory, while on cloudy days the instantaneous differences can be close to the entire peak power, as occurs during the afternoons of the 4th and 7th days. The previous outcomes are consistent with the fact that *FC* temporal resolution cannot predict power fluctuations, which occur in the range of minutes, but makes it possible to know, in some cases, when no severe power fluctuations will take place. Then, by identifying these moments, the algorithm could avoid unnecessary cycling as in Fig. 6.

By looking at MAE as a function of the minimum distance from *FC,* within the horizon *H,* to the instantaneous PV production limits ($\min\{|P_{FC,\max} - P_d(i)|, |P_c(i) - P_{FC,min}|\}$), an important result emerges (see Fig. 9): when the aforementioned metric is low (under 0.1) MAE is low (under 15%) and when it is close to its maximum, MAE reaches its maximum.

With the aid of a weight parameter (w), the proposed strategy could dynamically combine both strategies 2 and 3. When the metric $\mathbf{min}\{|P_{FC,\max} - P_d(i)|, |P_c(i) - P_{FC,min}|\}$ is high (the prediction is not reliable), Strategy 2 should take a prominent role in the control behavior (as can be seen in the figure, regardless of the value of H, MAE reaches its maximum for values above 0.5, therefore *FC* must be ignored for these values). While when the metric is low, the values of *FC* can be trusted. However, as is shown in Fig. 9, even for small values of the metric, the error does not disappear; therefore, a minimum weight ought to be given to Strategy 2 irrespectively of the metric. Finally, the weight (w) can be calculated as follows:

Table 1
Computed 5-second error metrics ($FC - P_{pv}$) through 2-year data series.

Mean AbsoluteError **MAE**	Mean Bias Error **MBE**	Standard DeviationError **SDE**	Root Mean Square Error**RMSE**
0.172	−0.0646	0.232	0.241

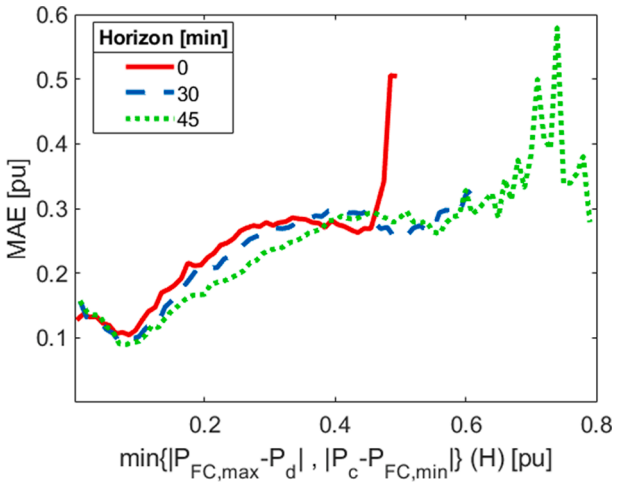

Fig. 9. Mean absolute error (MAE) for different horizons as function of $\min(|P_{FC,max} - P_d(i)|, |P_c(i) - P_{FC,min}|)$. Error $(P_{FC}(i) - P_{pv}(i))$ was evaluated along the entire data series of P_{pv} with 5-second sampling time.

$$w(i) = w_{min} + (1 - w_{min}) \cdot \frac{1}{0.5} \cdot \mathbf{min}\{|P_{FC,max} - Pd(i)|,\ |Pc(i) - P_{FC,min}|,\ 0.5\} \tag{13}$$

where w_{min} is the minimum weight applied to Strategy 2 (it could be zero depending on the forecasting quality).

The value of w can vary between w_{min} and the unity, when $\mathbf{min}\{|P_{FC,max} - P_d|, |P_c - P_{FC,min}|, 0.5\}$ varies from 0 to 0.5. If w is close to 1, *FC* is unreliable, and the opposite, when it is near w_{min}, *FC* can be considered to be reliable (as is shown in Fig. 9). Consequently, w is used for combining Strategy 2 and Strategy 3 in a weighted manner (Strategy 3w):

$$\begin{aligned} E^+_{3w} &= w \cdot E^+_2 + (1 - w) \cdot E^+_3 \\ E^-_{3w} &= w \cdot E^-_2 + (1 - w) \cdot E^-_3 \end{aligned} \tag{14}$$

where subscript 2 denotes the estimation provided by Strategy 2 (Eqs. (9) and (10)) and 3 is the one provided by Strategy 3 (Eqs. (12) and (10), computed in that order).

Finally, in order to prevent RR non-compliances due to lack of temporal resolution and/or prediction inaccuracies, a safety margin (E_s) is required at high and low energy storage levels. When the algorithm determines that it is not necessary to change the actual SOC ($E^*_b = E_b$ in Eq. (11)) an additional condition must be met: with the aim of preventing fully charged or discharged conditions, due to unforeseen fluctuation events, the stored energy must be sufficiently separated from those values (E_{max} and E_{min}, respectively). The modified SOC reference logic is described by the next pseudocode (Eq. (15)):

$$\begin{aligned}
&\textbf{if } E_b + E^+_{3w} > E_{max} \\
&\quad E^*_b = E_{max} - E^+_{3w} \\
&\textbf{elseif } \mathrm{E_b} - \mathrm{E^-_{3w}} < \mathrm{E}_{min} \\
&\quad E^*_b = E_{min} + E^-_{3w} \\
&\textbf{else} \\
&\quad \textbf{if } E_b > E_{max} - E_s \\
&\quad\quad E^*_b = E_{max} - E_s \\
&\quad \textbf{elseif } E_b < E_{min} + E_s \\
&\quad\quad E^*_b = E_{min} + E_s \\
&\quad \textbf{else} \\
&\quad\quad \mathrm{E^*_b} = \mathrm{E_b}
\end{aligned} \tag{15}$$

5.3. Strategy evaluation

A priori, the choice of the correct horizon (H) is not clear. For the strategy to function correctly, H must provide the control with sufficient time to reach the setpoint and, in the case of FC, absorb the temporal forecasting errors; additionally, the greater the proportional gain (K), the shorter the time required. Therefore, the method was tested for a wide range of horizons (1–60 [min]) and proportional gain values (0.1–6 [1/h]).

Two performance variables were obtained: cycling degradation (CyD) and number of days with RR violations. The results are plotted in Fig. 10. The proposal was tested for the two years of PV production data and an exigent ramp-rate constraint of 2%/min.

Fig. 10 shows different significant results. First: there is a region in which the number of RR violations is zero in the case of Strategy 3 (FC_p), it is approximately enclosed by $H > 15$[min] and $K > 2$[1/h]. It is significant that the minimum degradation partially coincides with the same region of full compliance. This means that PV smoothing, up to 2%/min, without RR violations, is feasible by knowing the maximum and minimum values within a horizon of 15 min, it does not mean the precise moment in which the highest and lowest values occur, but just their values.

As was expected, the using of Strategy 3 with FC leads to the appearance of a considerable number of RR non-compliances. The cycling degradation is reduced (compared to Strategy 2, see Table 5 in the next section), but not to the same extent as if FC_p were used. The regions of minimum degradation and non-compliances do not match, in fact, they are opposed.

Another relevant outcome is that the use of Strategy 3w can eliminate the RR violations in exchange for a slight increase in degradation (compared to Strategy 3 (FC_p)). Again, the regions of minimum RR non-compliance and degradation do not match; nevertheless, a well-balanced solution is possible, e.g. for $K = 3$ [1/h] and $H = 45$ [min] there are no RR violations and the expected degradation is about 2.85 [%/yr], which is 43% higher than the minimum degradation in the case of perfect prediction. The reason why Strategy 3w can reduce cycling, compared to Strategy 2, even if the prediction fails, is because the highlighted problem on Fig. 6 is solved. The irradiation during very overcast and clear days has a smooth evolution and the NWP methods can predict its shape and general behavior with sufficient precision. Then, the PV production can be forecasted with similar accuracy and, therefore, the control would not change the SOC reference unnecessarily. The same days and initial conditions in Fig. 6 are repeated in Fig. 11, but now using Strategy 3w, the improvement is evident.

Based on the results shown in Fig. 10, in order to compare strategy performance, the selected combination of parameters were $K = 3$[1/h], $H = 20$[min], for Strategy 3 with FC_p; and $K = 3$[1/h], $H = 45$[min], for Strategy 3w. The same example day used for illustrating the behavior of benchmark strategies is used to illustrate performance of the proposal in Fig. 12, showing the ideal condition of FC_p (Fig. 12(a)) and the progressive improvement from using Strategy 3 with FC (Fig. 12(b)) to the complete weighted method (Fig. 12(c)). The initial stored energy is the same for all cases. However, the evolution during the day differs. There is an evident lack of temporal resolution of FC in order to capture the fast power transitions, which causes a non-compliance in Fig. 12(b), when the battery reaches its full charge (indicated with a blue arrow). The weighted method (Fig. 12(c)) proves its efficiency in smoothing PV fluctuations with FC, a free publicly-available hourly sampled prediction; the battery evolution is quite similar to the one of Fig. 12(a), even if the two forecast series differ in quality.

Henceforth, '3' and '3w' will denote Strategy 3 with FC_p and Strategy 3w with FC, respectively.

6. Strategies comparison

In order to compare and evaluate performance, each strategy was simulated for the same restricted scenario (r = 2%/min). The battery efficiency was assumed to be constant but not symmetrical, i.e. in charge/discharge 90%/95% were used [36,37]. During simulations, no charge or discharge at night-time was allowed.

Despite the fact it does not depend on simulation but on ramp-rate limit, the required minimum storage was computed as an additional comparison between the strategies.

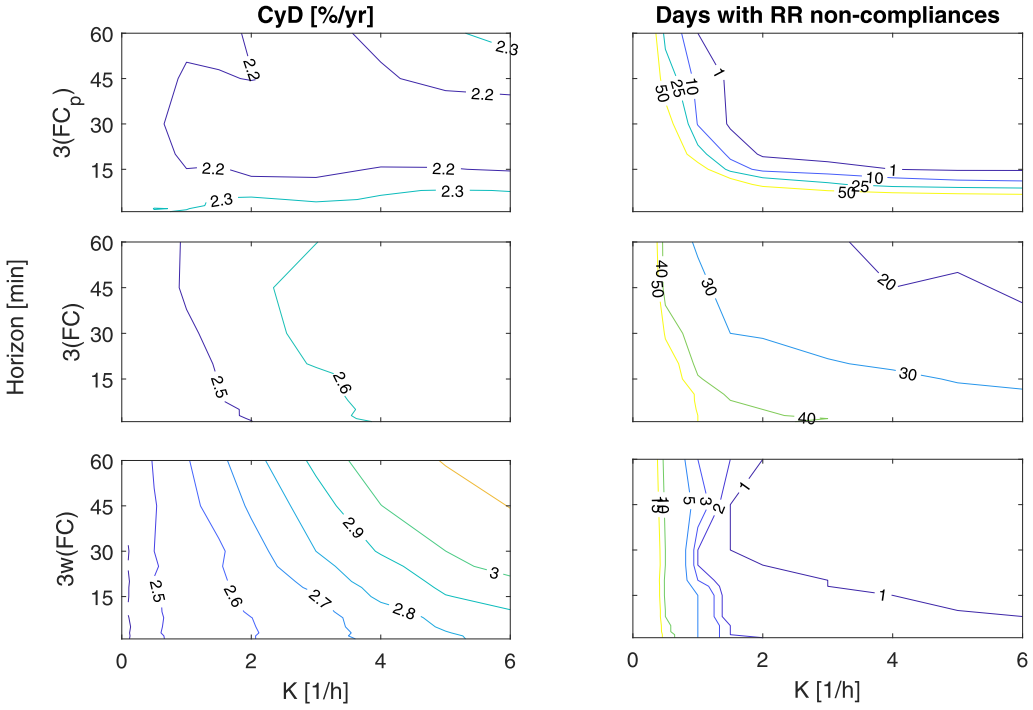

Fig. 10. Forecast horizon (H) and control gain (K) impact on performance of strategies 3 and 3w for different available forecasts. Left column: cycling degradation (CyD); right column: number of days with RR noncompliances. Ramp limit: $r = 2$%/min and, for Strategy 3w, $E_s = 0.2C_b$.

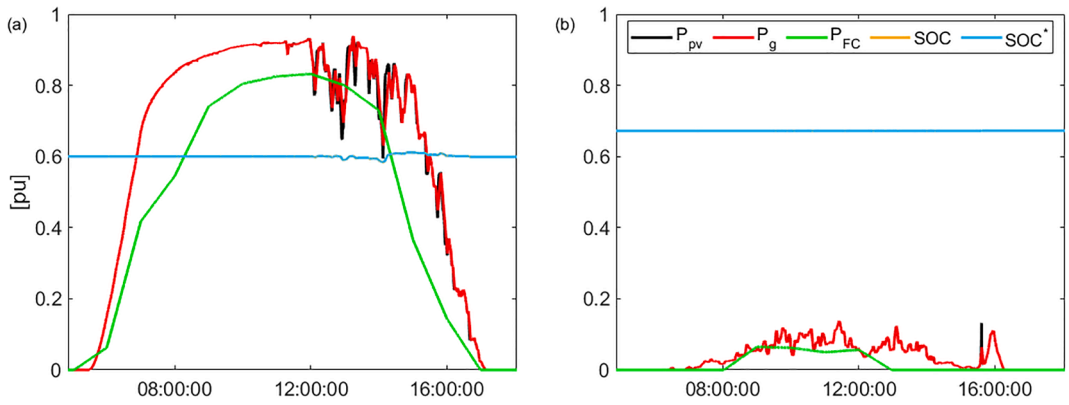

Fig. 11. Over-cycling reduction by using Strategy 3 and *FC* ($H = 15$ [min], $K = 3$[1/h]). (a) Unnecessary charge solved, (b) unnecessary discharge solved.

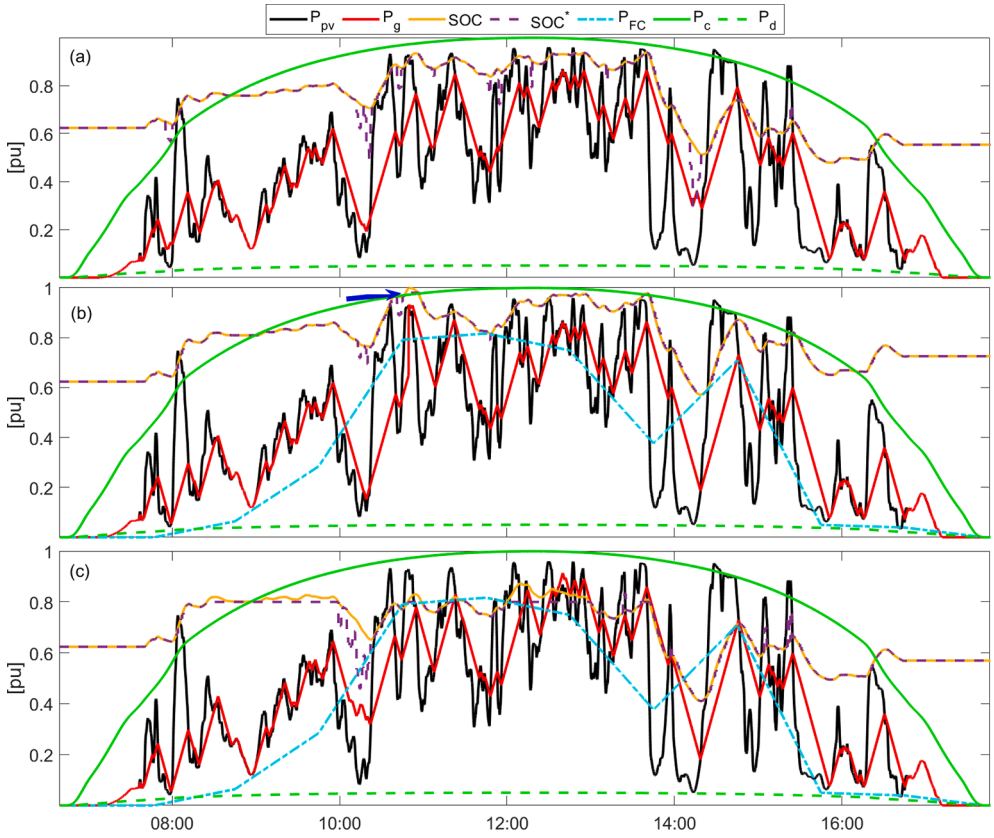

Fig. 12. Example of proposal behavior. (a) 3(FC_p), (b) 3(*FC*), (c) 3w (*FC*) with $E_s = 0.2 \cdot C_b$. In (a) forecasting is omitted as it is identical to P_{pv}.

6.1. Minimum capacity

The minimum capacity for each strategy is plotted as a function of the desired smoothing (r) in Fig. 13. The capacity required by strategies 2–3 (Eq. (8)) is lower than any other in every circumstance, however its advantage in terms of capacity is more significant (compared to Strategy 1, Eq. (7)) in low restricted scenarios, e.g. for RR limitations higher than 6%/min. On the other hand, Strategy 0 demands the higher capacity under any circumstances (Eq. (5)).

Despite the fact that Fig. 13 shows minimum storage limits for each strategy; the battery behavior introduces a further constraint. The full battery capacity should not be extracted as this would lead to a severe lifespan reduction, therefore, the total capacity must be higher. In this paper, for all strategies, the total capacity is considered to be 25% over the minimum one, which implies that the usable capacity represents 80% of total storage.

6.2. Charge/discharge power

Power cumulative distributions are shown in Fig. 14. The total time of use is included in hours and as a percentage of the two years. The reader should be aware that the frequencies of each strategy are linked to its own time of use.

Strategies 0 and 2 have a similar distribution but differ in their time of use. While for Strategy 0 it is 2850 h, that of Strategy 2 is 3512 h. Furthermore, among the strategies with no prediction, Strategy 0 is the one that uses its battery for fewer hours; in contrast, Strategy 1 exhibits severe usage (8057 h) with the highest frequencies in the entire power range.

On the other hand, the availability of PV power forecasting allows

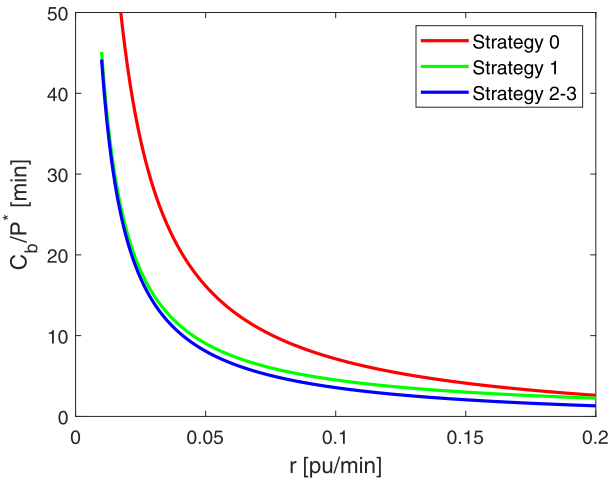

Fig. 13. Minimum capacity requirements for different strategies. Red: Strategy 0 (eq.5), green: Strategy 1 (Eq. (7)), blue: strategies 2–3 (Eq. (8), $\tau = 1$[min]). (For interpretation of the references to colour in this figure legend, the reader is referred to the web version of this article.)

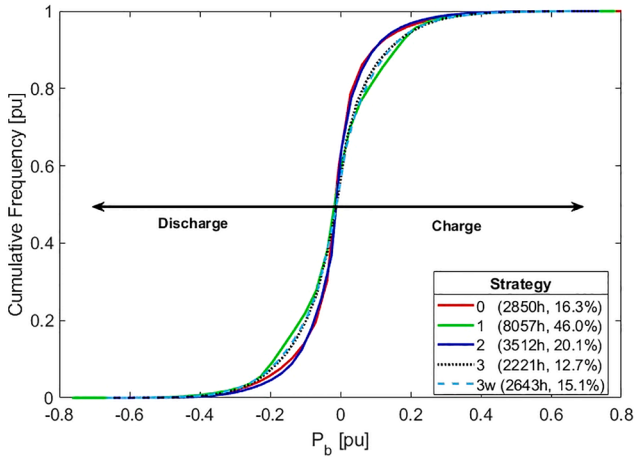

Fig. 14. Cumulative frequency distributions for different strategies. The box shows the amount of time (in 2 years) that $|P_b|$ is higher than 0, in hours and as percentage.

strategies 3 (2221 h) and 3w (2643 h) to outperform the benchmark ones. As was expected, the use of a hypothetical perfect prediction leads to the lowest operating time. However, the accuracy of the prediction is not a critical factor in terms of achieving a significant improvement: 3 and 3w show a difference of just 211 h per year and with practically identical distributions. Compared to Strategy 2, Strategy 3w reduces the temporal utilization by more than 800 h (400 each year).

6.3. Throughput energy

The energy handled by batteries is a natural consequence of the power distributions shown in Fig. 14. Table 2 presents the energy flow through the battery (E_t) with two metrics: the number of equivalent cycles, a measure of the battery degradation, which is the ratio between energy and twice the capacity ($E_t/2C_b$); and the ratio with the total photovoltaic energy (E_t/E_{pv}), useful for energy wastage analyses and for economic purposes.

Table 2
Throughput energy (E_t) managed by batteries of different strategies during two simulated years. Number of equivalent cycles ($E_t/2C_b$) and energy as fraction of total PV energy (E_t/E_{pv}).

Strategy	0	1	2	3	3w
$E_t/2C_b$[Eq.Cycles]	127	869	284	196	244
E_t/E_{pv}[%]	4.5	15	5.0	3.7	4.3

In terms of equivalent cycles and due to its high capacity, Strategy 0 produces the lowest number (127), which would lead to the lowest cycling degradation and, consequently, longest lifespan. As was expected, Strategy 1 causes battery over-cycling, which is far greater than any of the other strategies, on average, more than one equivalent cycle per day (869). Strategy 3w reduces the number of cycles of Strategy 2 by 40 (20 per year), the maximum reduction could be 44 cycles each year if perfect forecasting were available (Strategy 3).

On the other hand, in terms of total energy (E_t/E_{pv}), two facts emerge: firstly, forecasting strategies outperform any of the benchmark methods, irrespective of whether FC_p or FC are used. Secondly, the use of strategies 3 and 3w leads to comparable results: the energy flow is 25% higher for the weighted method in comparison to perfect forecast. Thus, the availability of a perfect forecast is not required in order to get a significant improvement.

If the energy losses (E_{loss}) related to ESS usage are estimated as follows:

$$E_{loss} = \left(1 - \eta_{pe}\left(\frac{\eta_c}{2} + \frac{\eta_d}{2}\right)\right)E_t \tag{16}$$

where E_t is the battery throughput energy (in pu), and η_{pe}, η_c and η_d are the efficiency of power electronics, charge and discharge, respectively. With a total efficiency of 90% ($\eta_c = 90\%$, $\eta_d = 95\%$ and$\eta_{pe} = 97\%$), according to the results shown in Table 2, strategies 0, 2, 3 and 3w would have insignificant losses, between 0.37% and 0.5% of total production; however, Strategy 1 would give a considerable loss of 1.5%.

Fig. 15 shows plots of the SOC evolution over three consecutive days as well as the PV power and predicted production. The results are consistent with those of Table 2. The characteristic over-cycling of Strategy 1 is evident; in the same way, the consequences of the pessimistic approach of Strategy 2 are clear (particularly on day one and two). It can be seen that strategies 3 and 3w behave in a similar way during clear and overcast days, even though there may be a few discrepancies produced by inaccuracies in power forecasting (as can be seen on the morning of the first day). Additionally, the positive effect of the weight parameter (Eq. (13)) can be noted: at first day morning, strategy 3w performs a charge that is several times less than that which would be produced by strategy 2. In addition, strategies 3 and 3w successfully avoid the heavy discharge that Strategy 2 produces at the beginning of the second day, avoiding excessive and unnecessary cycling.

Furthermore, the reduced cycling of Strategy 0 is illustrated, and also its energy flux which is higher than that of strategies 3 and 3w (as can be seen in Table 2). On the third day, in the early morning, there is an upward fluctuation that charges the batteries of all the strategies, the change in SOC is related to the amount of degradation. While for strategies 3 and 3w the change is close to 20%, for Strategy 0 it is almost 10%, due to its double capacity and, for the same amount of energy, the change in SOC of strategies 3-3w is twice that of Strategy 0. However, as can be seen in the zoom detail, Strategy 0 implies a higher energy flux because of the continuous attempt of its control loop to restore SOC to its reference value. Following the aforementioned fluctuation, the SOC of Strategy 3 evolves 'freely' with a slight increase in charge; in contrast, Strategy 0 tries to return the SOC to its setpoint with a discharge. The magnitude of the change in SOC is almost the same for both strategies (as can be seen with the aid of the scale on the zoom detail), therefore, the energy flux is almost twice for Strategy 0. The subsequent downward fluctuation, which discharges the batteries in all cases, is followed by a sharp upward fluctuation, in this case, the SOC variation of Strategy 0 is higher than that of Strategy 3 and practically the same as for Strategy

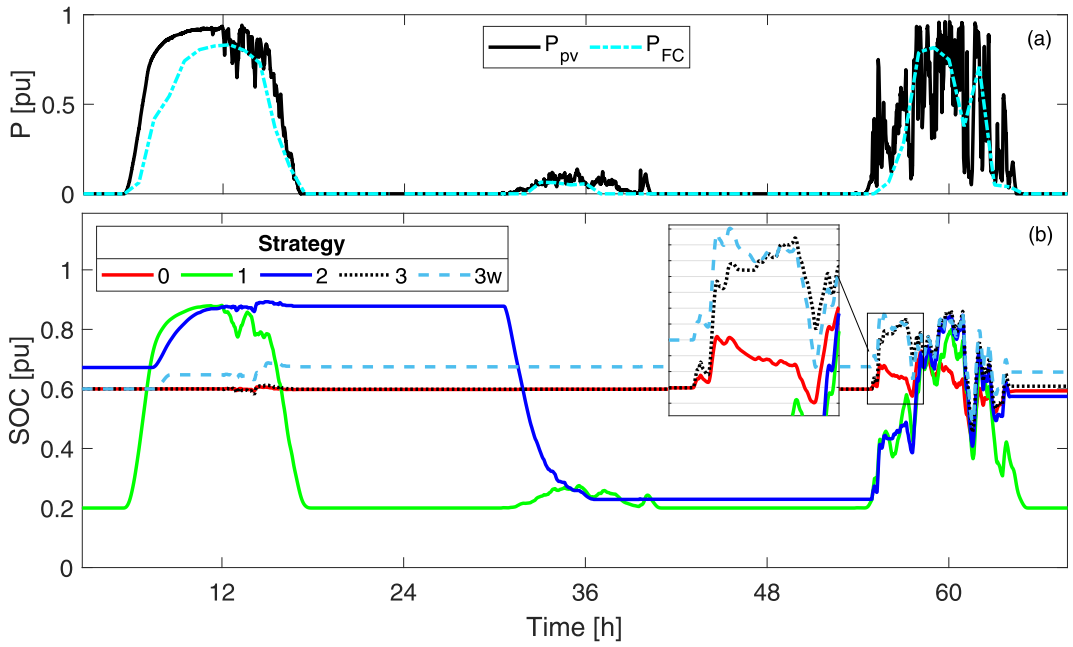

Fig. 15. SOC evolution during three consecutive days. (a) PV power and real NWP forecasting (*FC*). (b) Energy storage evolution during 3 simulated days.

3w, therefore, its throughput energy in this event doubles, at least, those of the strategies with forecasting.

Finally, it can be observed that, for the whole day, Strategy 3w behaves similar to Strategy 3, even if its forecasting is far from perfect (as can be seen at the top of Fig. 15). During that day, their SOC curves remain close at every moment in time and, at the end of the day, their SOCs are almost the same as at the beginning.

6.4. SOC distribution

SOC relative frequency distributions are shown in Fig. 16. These were scaled down in order to get a more general picture: the SOC_{min} (E_{min}) value is referred as 0 and SOC_{max} as 1 (E_{max}). As the reader will remember, the simulations were carried out with $E_{min}=0.2 \cdot C_b$ and $E_{max}=C_b$ and a total capacity of 1.25 times the minimum one (Fig. 13). Table 3 shows the minimum, mean and maximum values for each of the SOC distributions.

Strategy 0 has a clear mode in its reference value (50%), which is produced by the control loop. Strategy 1 has a clear bimodal shape, with its modes located close to SOC_{min} and SOC_{max}, that is due to the one-deep-cycle-per-day behavior; this pattern is very harmful for batteries because the high and low levels of SOC accelerate different degradation process [38,39,40]. Strategy 2 has an irregular behavior because of the variability of E_b^*. On the other hand, the distribution of Strategy 3 is not as disperse as Strategy 2 and their values are more centered, which means that the battery stays longer at intermediate SOC values. In the case of 3w the main region is limited between 0.2 and 0.8, which is produced by the safety margin (E_s) introduced in Eq. (15). Both of them reduce the mean value (compared to Strategy 2, see Table 3); finally, they exhibit similar extreme values (with an extremely low relative frequency) and are able to reduce the total range of SOC variation (compared to Strategy 2).

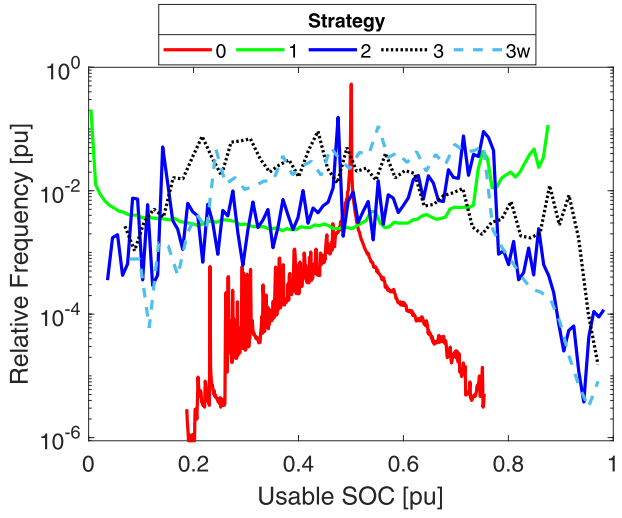

Fig. 16. Distributions of the SOC for different strategies over two simulated years. Y-axis is logarithmically scaled.

Table 3
Limits and mean values in SOC distributions of Fig. 16.

Strategy	0	1	2	3	3w
mean [%]	50	10	60	42	54
min [%]	19	0	3.6	6.1	7.5
max [%]	75	88	98	98	98

6.5. Degradation and expected life

Battery degradation is traditionally divided into two independent components: cycling degradation (*CyD*) and calendar degradation (*CaD*). Cycling degradation depends on the stress produced in the battery by all the conditions in which the charge and discharge processes occur, e.g. temperature, current, SOC variation and mean SOC [36,38,40,41,42,43]. Calendar degradation is produced when the battery is in standby, mainly by irreversible chemical parasitic processes that modify the original structure and reduce the amount of active material and its distribution [38,44]; it is principally affected by temperature and the stand-by SOC level.

According to the most common end of life criteria (EOL), a battery is considered "dead" when its capacity decays 20% from its original value. From this point onwards, the battery suffer an accelerated lack of performance [38,39,40].

Manufactures provide two different plots that make it possible to estimate the *CyD* and *CaD*. The first can be calculated by using the cycling life plot, which reproduces the number of identical cycles (*N*) that causes the battery to reach the EOL criteria as a function of depth of discharge (DOD). With the use of the rain-flow counting method [45,46], complex SOC series can be decomposed into a series of different cycles of equal DOD, and assuming that each of these groups degrade the battery in a proportional manner, the total *CyD* is obtained:

$$CyD = \frac{1}{T_{Data}} \sum_{i=1}^{80} \frac{N_i}{N_{I,max}} \tag{17}$$

where T_{Data} is the period covered by the data series, i is the cycle depth, N_i is the number of cycles computed by the method, and $N_{i,max}$ is the number of cycles defined by the cycling life plot. Fig. 17 is the curve used in this study.

The rain-flow counting method plus the cycling life plot is a fast procedure that is commonly used [25,27,48,49,50,51]. However, its accuracy is low due to the fact that the method underestimates the actual degradation: it does not consider the influence of current and temperature (it is common that available cycling life plots show results at 25 °C, an unrealistic condition in most applications). Given that Dufo-Lopez [50] found the ratio between estimated and experimental lifetime was between 2 and 3, all the *CyD* results in this work were corrected by a factor of 2.

The calendar degradation (*CaD*) can be estimated with the calendar life plot. It reproduces the years of expected life (up to the manufactur's warranty, generally 20 years) as a function of temperature and *SOC*. Fig. 18 shows the plot used.

The curves in Fig. 18 can be approximated to a function of the form: $a_1 exp(a_2 \cdot T)$ in which the coefficients a_1 and a_2 are obtained for each SOC level with a linear fitting ($a_i = m_i \cdot SOC[pu] + b_i$). Table 4 presents the coefficients that fit a_1 and a_2:

It is important to highlight the fact that, for SOC levels below 50% an extrapolation is computed in the parameters a_1 and a_2 (based on the data presented in Fig. 18), while an interpolation is made for upper values. With the use of the previous fitting it is possible to estimate the calendar degradation by taking into account the different vales of *SOC* within the frequency distribution (SOC_i), their relative frequencies (F_i) and the mean operational temperature (T):

$$CaD_i = \frac{1}{(m_1 \cdot SOC_i + b_1) exp(\{m_2 \cdot SOC_i + b_2\} \cdot T)} \tag{18}$$

$$CaD = \sum_{i=SOC_{min}}^{SOC_{max}} CaD_i \cdot F_i \tag{19}$$

Then, by using Eqs. (17) and (19), the expected battery lifespan is:

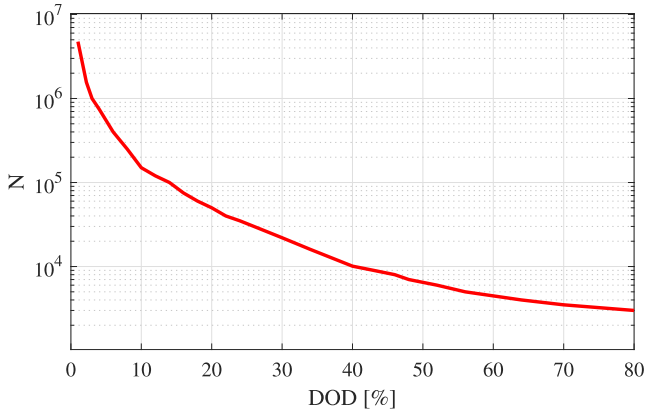

Fig. 17. Cycling life plot of a Li-ion battery [47] (DOD: depth of discharge, N: number of cycles). The y-axis is logarithmically scaled.

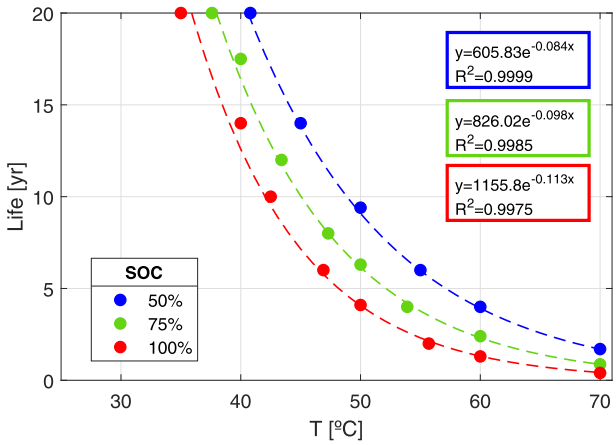

Fig. 18. Characteristic calendar degradation as a function of SOC and Temperature [52].

Table 4
Coefficients and R^2 for the linear fitting of a_1 and a_2

i	m_i	b_i	R^2
1	1045	58	0.973
2	−0.058	−0.054	0.999

Table 5
Comparative cycling degradation (*CyD*), calendar degradation (*CaD*) and expected life for Li-ion batteries depending on different strategies.

Strategy	0	1	2	3	3w
CyD [%/yr]	0.961	22.1	4.7	2.18	2.85
CaD [%/yr]	3.15	3.72	3.65	3.25	3.40
Expected life [yr]	24.3	3.87	12.0	18.4	16.0

$$Life[yr] = \frac{1}{CyD + CaD} \tag{20}$$

The result of *CyD*, *CaD* and expected life is presented in Table 5. In order to calculate *CaD*, a mean temperature of 35 °C was assumed. The results are consistent with those in previous sections. As was expected, Strategy 0 implies a higher battery longevity compared to other strategies, due to its limited number of equivalent cycles. Strategy 1 has a poor expected lifespan as a result of its intrinsic over-cycling behavior. Prediction-based strategies can reduce *CyD* by 40%, in comparison to Strategy 2, and can almost reach the entire life of the project, irrespective of whether FC_p is used or not. The difference between strategies 3 and 3w, in terms of expected life, is close to 2.4 years.

6.6. Levelized cost of energy (LCOE)

Based on the expected life, which is affected by all the preceding parameters, the number of battery replacements is obtained. It is then possible to compute the aggregated cost of the energy produced by the PV project. A metric usually used for comparative purposes is the levelized cost of energy (LCOE) [53,54,55], which considers the entire duration of the project. It is defined as:

$$LCOE = \frac{I_{0,pv} + I_{0,b} + \sum_{k=1}^{N} I_k}{\sum_{k=1}^{N} E_k (1+r)^{-k}} \tag{21}$$

where:

- $I_{0,pv}$ is the PV cost acquisition.
- $I_{0,b}$ is the cost of initial battery acquisition.

- k is the year of the project under consideration.
- N is the project's duration. In this study, we consider a 20-year PV project.
- I_k is the cost associated with the k-th year. It ought to include: capital and operational expenditures (CAPEX and OPEX, respectively).
- E_k is the energy production during the k-th year.
- r is the discount rate.

The parameters used to compute the LCOE are shown in Table 6.

Table 7 shows the results of the LCOE computation. As a reference, the case with no PV smoothing is also included. The base comparison reveals Strategy 3 to be the most cost-effective among the strategies analyzed with an LCOE of 66.7$/MWh. Although it does not have a perfect forecasting, Strategy 3w would imply a slight LCOE increase (67.1$/MWh). The cost increases, compared to the plant with no smoothing, would be 28% and 28.8%, for strategies 3 and 3w respectively. Therefore, perfect prediction is not a hard requirement for the proposed control method, its hypothetical availability could reduce the LCOE increase to an insignificant 0.8% or 0.4 $/MWh.

Even though Strategy 0 is the strategy with the highest expected lifespan, it increases LCOE in 48.4%, almost twice the increase of Strategy 3w. This is due to the fact that, at present prices, Strategy 0 acquires twice the capacity of the method proposed and, although Strategy 3w would demand a battery replacement, so both of them acquire the same amount of storage, such replacement for Strategy 3w would be postponed until the 17th year, involving an expected cost fade in batteries from 550 to 230 $/kWh.

It is noteworthy that the inclusion of an ESS with demanding smoothing requirements (2%/min) can almost double the LCOE, if an inadequate control strategy is selected (as in the case of Strategy 1).

7. Conclusion

This work presents a novel ramp-rate control strategy that has the ability to operate with minimum storage requirement and uses PV power forecasting in order to reduce the battery cycling and therefore, increase its lifespan. The strategy was designed to be able to work with real publicly-available PV power prediction and deal with its intrinsic inaccuracies and lack of temporal resolution. Furthermore, the strategy can be extrapolated to other plant sizes and locations following the battery size procedure and using the same control parameters (in per unit system).

The proposed solution was compared to three benchmark strategies and their performances were analyzed in terms of minimum storage requirement, battery power distribution, battery throughput energy, SOC distribution, degradation, expected life and levelized cost of energy (LCOE).

The proposed method outperforms the benchmark strategies in terms time of use and amount of throughput energy. For a demanding constraint of 2%/min, the simulations show that the proposal would use the battery for only 15.1% of the total time and that the energy passing through it would be 4.3% of the total available. These values are close to the performance limit of the strategy, which would be obtained with a hypothetical perfect prediction: 12.7% for the usage time and 3.7% for the amount of energy.

The results of the LCOE analysis showed the proposed scheme to be the most cost-effective one. The increase produced by the PV smoothing system is 28.8%, compared to a plant with no smoothing capabilities, while benchmark strategies were between 31% and 95.8%. The proposed strategy is capable of smoothing PV fluctuations and, at the same time, maintaining the price competitiveness of PV power production, which guaranties that the ramp-rate limitations imposed by the TSOs will not be a major concern for PV generation.

Table 6
Input parameters for the LCOE calculation.

Parameter	Value	Source
PV plant set up cost [$/kWp]	660	[56]
ESS cost [$/kWh]	550	[3,23]
OPEX/$I_{0,pv}$ [%/yr]	3	[57,58]
ESS cost reduction [$/kWh.yr]	20	[23,37]
Discount rate [%/yr]	4	[32]
PV panels degradation [%/yr]	0.25	[59]
Project lifetime [yr]	20	[32]
ESS charge efficiency [%]	90	[60,61]
ESS discharge efficiency [%]	95	[60,61]
ESS power electronics [%]	97	Own assumption
Initial Capacity Factor (CF) [%]	20.6	Own assumption*

* Due to its 1-axis trackers and its exceptional location, the CF at Amaraleja PV plant is higher than 25%, but the current trend in PV is the use of fixed modules; therefore, a more realistic value was assumed.

Table 7
LCOE comparative results.

Strategy	**No smoothing**	**0**	**1**	**2**	**3**	**3w**
$I_{0,pv} + I_{0,b}$[M$]	29.7	48.9	40.7	39.1	39.1	39.1
Battery replacements	–	0	5	1	1	1
I_k [M$]	17.8	17.8	50.9	23.1	21.4	21.8
$\sum E_k(1+r)^{-k}$[GWh]	912	905	898	907	908	908
LCOE [$/MWh]	**52.1**	**77.3**	**102**	**68.6**	**66.7**	**67.1**
Δ LCOE [%]	**–**	**48.4**	**95.8**	**31.7**	**28.0**	**28.8**

CRediT authorship contribution statement

A. Gonzalez-Moreno: Formal analysis, Writing – original draft, Conceptualization, Visualization. **J. Marcos:** Conceptualization, Writing – review & editing, Supervision. **I. de la Parra:** Data curation, Methodology. **L. Marroyo:** Conceptualization, Writing – review & editing, Supervision.

Declaration of Competing Interest

The authors declare that they have no known competing financial interests or personal relationships that could have appeared to influence the work reported in this paper.

Acknowledgements

The authors would like to thank ACCIONA for authorizing measurements at its PV plants and for the helpful collaboration of its staff. Likewise, we would like to acknowledge the support of the Spanish State Research Agency (AEI) under grants PID2019111262RB-I00 and PID2019-110816RB-C21. Open access funding provided by Universidad Pública de Navarra.

References

[1] REN21. Renewables 2019: Global Status Report, REN21 Secretariat, Paris; 2019.
[2] LAZARD. Lazard's Levelized Cost of Energy Analysis—Version 13.0; 2019.
[3] LAZARD. Lazard's Levelized Cost of Storage Analysis—Version 5.0; 2019.
[4] EIA. Levelized Cost and Levelized Avoided Cost of New Generation Resources in the Annual Energy Outlook 2020, U.S. Energy Information Administration; 2020.
[5] Jewell W, Ramakumar R. The effects of moving clouds on electric utilities with dispersed photovoltaic generation. IEEE Trans Energy Convers 1987;EC-2 (4): 570–6. https://doi.org/10.1109/TEC.1987.4765894.
[6] Shah R, Mithulananthan N, Bansal R, Ramachandaramurthy V. A review of key power system stability challenges for large-scale PV integration. Renew Sustain Energy Rev 2015;41:1423–36. https://doi.org/10.1016/j.rser.2014.09.027.
[7] Marcos J, Marroyo L, Lorenzo E, Alvira D, Izco E. Power output fluctuations in large scale pv plants: one year observations with one second resolution and a derived analytic model. Prog Photovolt Res Appl 2011;19(2):218–27. https://doi.org/10.1002/pip.1016.

[8] Marcos J, Marroyo L, Lorenzo E, Alvira D, Izco E. From irradiance to output power fluctuations: the PV plant as a low pass filter. Prog Photovolt Res Appl 2011;19(5): 505–10. https://doi.org/10.1002/pip.1063.

[9] Marcos J, Storkël O, Marroyo L, Garcia M, Lorenzo E. Storage requirements for PV power ramp-rate control. Sol Energy 2014;99:28–35. https://doi.org/10.1016/j.solener.2013.10.037.

[10] de la Parra I, Marcos J, Garcia M, Marroyo L. Control strategies to use the minimum energy storage requirement for PV power ramp-rate control. Sol Energy 2015;111: 332–43. https://doi.org/10.1016/j.solener.2014.10.038.

[11] Lappalainen K, Valkealahti S. Output power variation of different PV array configurations during irradiance transitions caused by moving clouds. Appl Energy 2017;190:902–10. https://doi.org/10.1016/j.apenergy.2017.01.013.

[12] Lappalainen K, Wang GC, Kleissl J. Estimation of the largest expected photovoltaic power ramp rates. Appl Energy 2020;278:115636. https://doi.org/10.1016/j.apenergy.2020.115636.

[13] Chalmers S, Hitt M, Underhill J, Anderson PM, Vogt PL, Ingersoll R. The effect of photovoltaic power generation on utility operation. IEEE Trans Power Appar Syst 1985;PAS-104 (3):524–30. https://doi.org/10.1109/TPAS.1985.318968.

[14] Cabrera-Tobar A, Bullich-Massague E, Aragues-Peñalba M, Gomis-Bellmunt O. Review of advanced grid requirements for the integration of large scale photovoltaic power plants in the transmission system. Renew Sustain Energy Rev 2016;62:971–87. https://doi.org/10.1016/j. rser.2016.05.044.

[15] Seck GS, Krakowski V, Assoumou E, Maïzi N, Mazauric V. Embedding power system's reliability within a long-term energy system optimization model: linking high renewable energy integration and future grid stability for France by 2050. Appl Energy 2020;257:114037. https://doi.org/10.1016/j.apenergy.2019.114037.

[16] PREPA. Puerto Rico Electric Power Authority Minimum Technical Requirements for Photovoltaic Generation (PV) Projects, Puerto Rico Electric Power Authority; 2012.

[17] CRE. ANEXO 3: Requerimientos Tecnicos Para Interconexion De Centrales Solares Fotovoltaicas Al Sistema Electrico Nacional, in: Reglas generales de interconexion al sistema electrico nacional, Comision Reguladora de Energia, Mexico; 2014.

[18] CNE. Norma Tecnica de Seguridad y Calidad de Servicio, Chile; 2015.

[19] AEMC. National Electricity Rules version 150, Australian Energy Market Commission, Australia; 2019.

[20] NERSA, Grid connection code for renewable power plants (RPPs) connected to the electricity transmission system (TS) or the distribution system (DS) in South Africa. Version 3.0, National Energy Regulator of South Africa, South Africa, 2019.

[21] Shivashankar S, Mekhilef S, Mokhlis H, Karimi M. Mitigating methods of power fluctuation of photovoltaic (PV) sources – a review. Renew Sustain Energy Rev 2016;59:1170–84. https://doi.org/10.1016/j.rser.2016.01.059.

[22] Jiang Y, Fletcher J, Burr P, Hall C, Zheng B, Wang D-W, et al. Suitability of representative electrochemical energy storage technologies for ramp-rate control of photovoltaic power. J Power Sources 2018;384:396–407. https://doi.org/10.1016/j.jpowsour.2018.03.013.

[23] Curry C. Lithium-ion battery costs and market. Bloomberg New Energy Finance; 2017.

[24] Perez R, Hoff T, Dise J, Chalmers D, Kivalov S. The cost of mitigating short-term PV output variability. Energy Proc 2014;57:755–62. https://doi.org/10.1016/j.egypro.2014.10.283.

[25] Beltran H, Tomas Garcia I, Alfonso-Gil JC, Perez E. Levelized cost of storage for li-ion batteries used in PV power plants for ramp-rate control. IEEE Trans Energy Convers 2019;34(1):554–61.

[26] Sukumar S, Marsadek M, Agileswari K, Mokhlis H. Ramp-rate control smoothing methods to control output power fluctuations from solar photovoltaic (PV) sources—a review. J Storage Mater 2018;20:218–29. https://doi.org/10.1016/j.est.2018.09.013.

[27] Marcos J, de la Parra I, Garcia M, Marroyo L. Control strategies to smooth short-term power fluctuations in large photovoltaic plants using battery storage systems. Energies 2014;7(10):6593–619. https://doi.org/10.3390/en7106593.

[28] Puri A. Optimally smoothing output of PV farms. In: 2014 IEEE PES general meeting|conference exposition; 2014. p. 1–5. doi:10.1109/PESGM.2014.6939029.

[29] Saleh M, Meek L, Masoum MAS, Abshar M. Battery-less short-term smoothing of photovoltaic generation using sky camera. IEEE Trans Ind Inf 2018;14(2):403–14. https://doi.org/10.1109/TII.2017.2767038.

[30] Chen X, Du Y, Wen H, Jiang L, Xiao W. Forecasting-based power ramp-rate control strategies for utility-scale pv systems. IEEE Trans Ind Electron 2019;66(3): 1862–71. https://doi.org/10.1109/TIE.2018.2840490.

[31] Wen H, Du Y, Chen X, Lim E, Wen H, Jiang L, et al. Deep learning based multistep solar forecasting for PV ramp-rate control using sky images. IEEE Trans Ind Inf 2021;17(2):1397–406.

[32] Cires E, Marcos J, de la Parra I, Garcıa M, Marroyo L. The potential of forecasting in reducing the LCOE in PV plants under ramp-rate restrictions. Energy 2019;188: 116053. https://doi.org/10.1016/j. energy.2019.116053.

[33] Almeida MP, Muñoz M, de la Parra I, Perpiñan O. Comparative study of PV power forecast using parametric and nonparametric PV models. Sol Energy 2017;155: 854–66.

[34] Braco E, San Martín I, Berrueta A, Sanchis P, Ursúa A. Experimental assessment of cycling ageing of lithium-ion second-life batteries from electric vehicles. J Storage Mater 2020;32:101695.

[35] COPERNICUS. Soda-pro – cams mcclear service for irradiation under clear-sky. <https://www.soda-pro.com/web-services/radiation/cams-mcclear>.

[36] Alam MJE, Saha TK. Cycle-life degradation assessment of battery energy storage systems caused by solar PV variability. In: 2016 IEEE Power and Energy Society General Meeting (PESGM), IEEE, Boston, MA, USA; 2016. p. 1–5. doi:10.1109/PESGM.2016.7741532.

[37] IRENA. Electricity storage and renewables: Costs and markets to 2030, Tech. rep., International Renewable Energy Agency, Abu Dhabi; 2017.

[38] Ecker M, Nieto N, Käbitz S, Schmalstieg J, Blanke H, Warnecke A, et al. Calendar and cycle life study of Li(NiMnCo)O2-based 18650 lithium-ion batteries. J Power Sources 2014;248:839–51. https://doi.org/10.1016/j.jpowsour.2013.09.143.

[39] Schmalstieg J, Käbitz S, Ecker M, Sauer DU. A holistic aging model for Li(NiMnCo) O2 based 18650 lithium-ion batteries. J Power Sources 2014;257:325–34. https://doi.org/10.1016/j.jpowsour.2014.02.012.

[40] Baghdadi I, Briat O, Deletage J-Y, Gyan P, Vinassa J-M. Lithium battery aging model based on Dakin's degradation approach. J Power Sources 2016;325:273–85. https://doi.org/10.1016/j. jpowsour.2016.06.036.

[41] Liaw BY, Jungst RG, Nagasubramanian G, Case HL, Doughty DH. Modeling capacity fade in lithium-ion cells. J Power Sources 2005;140(1):157–61. https://doi.org/10.1016/j.jpowsour.2004.08.017.

[42] Wang J, Liu P, Hicks-Garner J, Sherman E, Soukiazian S, Verbrugge M, et al. Cycle-life model for graphite-LiFePO4 cells. J Power Sources 2011;196(8):3942–8. https://doi.org/10.1016/j.jpowsour.2010.11.134.

[43] Stiaszny B, Ziegler JC, Krauß EE, Schmidt JP, Ivers-Tiffee E. Electrochemical characterization and post-mortem analysis of aged LiMn2O4–Li(Ni0.5Mn0.3Co0.2) O2/graphite lithium ion batteries. Part I: Cycle aging. J Power Sources 2014; 251: 439–50. doi:10.1016/j. jpowsour.2013.11.080.

[44] Stiaszny B, Ziegler JC, Krauß EE, Zhang M, Schmidt JP, Ivers-Tiffee E. Electrochemical characterization and post-mortem analysis of aged LiMn2O4–NMC/graphite lithium ion batteries part II: Calendar aging. J Power Sources 2014;258:61–75. https://doi.org/10.1016/j.jpowsour.2014.02.019.

[45] Matsuishi M, Endo T. Fatigue of metals subjected to varying stress. Japan Soc Mech Eng, Fukuoka 1968;68(2):37–40.

[46] McInnes C, Meehan P. Equivalence of four-point and three-point rainflow cycle counting algorithms. Int J Fatigue 2008;30(3):547–59. https://doi.org/10.1016/j.ijfatigue.2007. 03.006.

[47] SAFT. Intensium Flex (Document N° 21535-2-0708); 2008.

[48] Schaltz E, Khaligh A, Rasmussen PO. Influence of battery/ultracapacitor energy-storage sizing on battery lifetime in a fuel cell hybrid electric vehicle. IEEE Trans Veh Technol 2009;58(8):3882–91. https://doi.org/10.1109/TVT.2009.2027909.

[49] Gee AM, Robinson FVP, Dunn RW. Analysis of battery lifetime extension in a smallscale wind-energy system using supercapacitors. IEEE Trans Energy Convers 2013;28(1):24–33. https://doi.org/10.1109/TEC.2012.2228195.

[50] Dufo-Lopez R, Lujano-Rojas JM, Bernal-Agustın JL. Comparison of different lead–acid battery lifetime prediction models for use in simulation of stand-alone photovoltaic systems. Appl Energy 2014;115:242–53. https://doi.org/10.1016/j.apenergy.2013.11.021.

[51] de la Parra I, Marcos J, Garcıa M, Marroyo L. Improvement of a control strategy for PV power ramp-rate limitation using the inverters: reduction of the associated energy losses. Sol Energy 2016;127:262–8. https://doi.org/10.1016/j.solener.2016.01.032.

[52] SAFT. Lithium-ion battery life (Document N° 21893-2-0514); 2014.

[53] Lai CS, McCulloch MD. Levelized cost of electricity for solar photovoltaic and electrical energy storage. Appl Energy 2017;190:191–203. https://doi.org/10.1016/j.apenergy.2016.12.153.

[54] Lai CS, Jia Y, Xu Z, Lai LL, Li X, Cao J, et al. Levelized cost of electricity for photovoltaic/biogas power plant hybrid system with electrical energy storage degradation costs. Energy Convers Manage 2017;153:34–47. https://doi.org/10.1016/j.enconman.2017.09.076.

[55] Marcos J, De la Parra I, Cires E, Wang G, Garcia M, Marroyo L. Ramp-rate control in large PV plants: battery vs. short-term forecast. In: 2018 20th European conference on power electronics and applications (EPE'18 ECCE Europe); 2018. p. P.1–P.6, iSSN: null.

[56] Kost C, Shammugam S, Jülch V, Nguyen H-T, Schlegl T. Levelized cost of electricity- renewable energy technologies; 2018.

[57] Branker K, Pathak MJM, Pearce JM. A review of solar photovoltaic levelized cost of electricity. Renew Sustain Energy Rev 2011;15(9):4470–82. https://doi.org/10.1016/j.rser.2011.07.104.

[58] Hernandez-Moro J, Martinez-Duart JM. Analytical model for solar PV and CSP electricity costs: present LCOE values and their future evolution. Renew Sustain Energy Rev 2013;20:119–32. https://doi.org/10.1016/j.rser.2012.11.082.

[59] Pascual J, Berrueta A, Marcos J, Garcia M, Marroyo L. On the on-site measurement of the degradation rate of crystalline silicon PV modules at plant level. In: 2018 IEEE international conference on environment and electrical engineering and 2018 IEEE industrial and commercial power systems Europe (EEEIC/I CPS Europe); 2018. p. 1–5. doi:10.1109/EEEIC.2018.8493718.

[60] Kang J, Yan F, Zhang P, Du C. A novel way to calculate energy efficiency for rechargeable batteries. J Power Sources 2012;206:310–4.

[61] Bobanac V, Basic H, Pandzic H. Determining lithium-ion battery one-way energy efficiencies: influence of C-rate and coulombic losses. In: IEEE EUROCON 2021 – 19th international conference on smart technologies; 2021. p. 385–9. doi:10.1109/EUROCON52738.2021.9535542.